Journal of Shipping and Ocean Engineering 6 (2017) 223-232
doi 10.17265/2159-5879/2017.06.001

naoe-FOAM-SJTU Solver for Numerical Study of Vortex-Induced Motions of a Buoyancy Can in Currents

XIE Kangdi, ZHAO Weiwen and WAN Decheng

Collaborative Innovation Center for Advanced Ship and Deep-Sea Exploration, State Key Laboratory of Ocean Engineering, School of Naval Architecture, Ocean and Civil Engineering, Shanghai Jiao Tong University, Shanghai 201306, China

Abstract: This paper presents 3D (three-dimensional) CFD (computational fluid dynamic) simulation to analyse the FIR (flow-induced response) especially the yaw motion of a buoyancy can. The numerical cases are conducted with a buoyancy can under different reduced velocities utilizing our in-house code naoe-FOAM-SJTU, a solver based on the open source toolkit OpenFOAM. SST-DDES (shear-stress transport-delayed detached-eddy simulation) model is applied to handle the flowseparation and overset grid method is utilized to solve a large amplitude 6-DOF (6 degrees of freedom) motions. Free decay test and VIM (vortex-induced motion) test are built numerically. In VIM cases, the responses of trajectory, amplitude, frequency are calculated in a series of reduced velocities. With the increase of reduced velocity, yaw frequency is increased, which is similar to surge and sway frequency. And yaw frequency is equal to the sway frequency, which is consistent with experimental results. Furthermore, comparing two cases, one fixed in rotation and the other one free in rotation, it can be concluded that release in the degree of rotation can decrease the sway amplitude but make no difference in the surge amplitude.

Key words: Buoyancy can, DDES, overset grid, vortex-induced motions.

1. Introduction

Buoyancy cans in typical cylindrical shape are widely applied in deep-water fields to tension a riser and keep it vertical [1]. Flow over a buoyancy can induces an alternating vortex shedding, which leads to the surge, sway and yaw motions. Recent studies concentrate on the motion characteristics of Spar platforms and semi-submersible platforms, while few researchers push forward the investigation into the VIM (vortex-induced motion) phenomenon especially the yaw motion of the typical cylindrical object. Therefore, the buoyancy can in typical cylindrical shape is a suitable object to reveal the mechanism of VIM phenomenon.

Methods in investigating the VIM phenomenon can be normally divided into two categories, model test and numerical simulation. A lot of model tests [2, 3] to comprehend the mechanism of VIM have been delivered. Govardhan and Williamson [4] delivered a model test of a tethered sphere to investigate the VIM phenomenon. They found that the tethered sphere oscillated vigorously in a large range of velocities and the RMS (root-mean-square) amplitude is independent of the length. De Wilde [5] was one of the earliest researchers in the VIM study of FRS (free standing riser system) containing the buoyancy can. His investigation illustrated the components of FRS and set up a model test containing a buoyancy can, cables, risers, which demonstrates the relationship between vibration model and the current velocity, the trajectory of the riser in X-Y plane. Due to the complexity of the model test system, De Wilde can only get some basic information about VIM phenomenon observed by other researchers. Therefore, it is inappropriate to investigate complex systems from the beginning. To simplify the FRS and investigate the mechanism of VIM phenomenon, KANG et al. [6, 7] present an

Corresponding author: WAN Decheng, Ph.D., professor, research fields: ship performance, ocean engineering, ship hull form optimization, numerical simulations of floating offshore wind turbines, vortex-induced vibration of riser, vortex-induced motion of platform, meshfree particle method.

experimental investigation on 6-DOF (6 degrees of freedom) vortex-induced motion response of a tethered buoyancy can under conditions of different tether lengths and illustrate the relationship between the yaw motion and the motion in the inline and cross flow directions.

Numerical simulation is also an effective method to investigate the VIM issues, and numerical tests have fit well with the experimental results in vortex-induced motion of the platform. Etienne and Fontaine [8] conducted a 2D (two-dimensional) numerical simulation to study the motion trajectory of the cylinder after releasing the rotational degree of freedom. Minguez et al. [9, 10] presented a slender buoyancy can flow-induced response at high Reynolds number and 2D CFD (computational fluid dynamic) model is built to investigate the yaw responses of the buoyancy can.

The aim of this paper is to present 3D CFD model to analyse the FIR (flow-induced response) especially the yaw motion of a buoyancy can and illustrate the relationship between the yaw motion and the motion in the inline and cross flow directions. Furthermore, the influence level of release in the degree of rotation is also illustrated in this paper.

2. Numerical Methods

2.1 Governing Equations

In this paper, a DDES (delayed detached-eddy simulation) method based on the SST (shear-stress transport) model is used to simulate the turbulence detached flow during a large range of high Reynolds numbers [11]. SST-DDES is a hybrid RANS (Reynolds-Averaged Navier-Stokes)-LES (large eddy simulation) method. It utilizes sub-grid scale model to handle the flow in the free shear flow area far away from wall, and employs RANS's SST model to solve the flow in the boundary layer near wall and other areas. This can guarantee the accuracy of LES solution, and reduce the amount of calculation in the near-wall region of the boundary layer. For incompressible viscous fluids, the continuity equation and momentum equation can be expressed as:

$$\frac{\partial \overline{u}_i}{\partial x_i} = 0 \tag{1}$$

$$\frac{\partial \overline{u}_i}{\partial t} + \frac{\partial \overline{u}_j \overline{u}_i}{\partial x_j} = \frac{\partial \overline{P}}{\partial x_i} + \frac{\partial}{\partial x_j}\left[v\left(\frac{\partial \overline{u}_i}{\partial x_j} + \frac{\partial \overline{u}_j}{\partial x_i} \right) \right] - \frac{\partial \tau_{ij}}{\partial x_j} \tag{2}$$

where, v is the molecular viscosity, τ_{ij} is the Reynolds stress or sub-grid stress tensor. According to the Boussinesq hypothesis, τ_{ij} can be expressed as:

$$\tau_{ij} = \frac{2}{3}\delta_{ij}k - v_t\left(\frac{\partial \overline{u}_i}{\partial x_j} + \frac{\partial \overline{u}_j}{\partial x_i} \right) \tag{3}$$

SST-DDES turbulence model assumes that the turbulent viscosity v_t can be expressed as a function of turbulent kinetic energy k, turbulence dissipation rate ω and velocity strain S [12]:

$$v_t = \frac{a_1 k}{\max(a_1\omega, SF_2)} \tag{4}$$

where, k and ω can be obtained by solving the corresponding transport equation:

$$\frac{\partial k}{\partial t} + \frac{\partial (u_j k)}{\partial x_j} = \tilde{G} - \frac{k^{\frac{2}{3}}}{l_{DDES}} + \frac{\partial}{\partial x_j}\left[(v + \alpha_k v_t)\frac{\partial k}{\partial x_j} \right] \tag{5}$$

$$\frac{\partial \omega}{\partial t} + \frac{\partial (u_j \omega)}{\partial x_j} = \gamma S^2 - \beta\omega^2 + \frac{\partial}{\partial x_j}\left[(v + \alpha_\omega v_t)\frac{\partial \omega}{\partial x_j} \right] - (1 - F_1) CD_{k\omega} \tag{6}$$

The l_{DDES} in Eq. (5) is the mixed length, which is the switch that controls the transformation between LES and RANS model [11].

2.2 Overset Grid

Traditional dynamic grid method is difficult to deal with a large amplitude 6-DOF motion problem, and the overset grid method is one of the effective ways to solve such problems. In this paper, oversetting grid program Suggar ++ [13] is applied to calculate the DCI (domain connectivity information). DCI mainly

consists of cell information (hole cell, interpolated cell, donor cell, orphan cell) and interpolated weight coefficient. Naoe-FOAM-SJTU solver [14, 15] runs Open FOAM and Suggar ++ respectively in different processes to achieve full parallelization of the flow field solution and overset grid digging interpolated calculation. Grid movement among different processes and DCI information exchange are through the MPI (message passing interface). The detailed information concerning the coupling of Open FOAM and Suggar ++ can be found in SHEN et al.'s [16] paper.

3. Computational Model

3.1 Parameter Definition

In general, buoyancy cans with 6-DOF under the constraint of the mooring system will induce significant surge, sway and yaw motions. In this paper, surge is assumed to be in line with the flow, sway is the motion in the transverse direction to the flow, and yaw is the rotation in z-axis.

The characteristics of VIM are mainly determined by the reduced velocity U_r, the Reynolds number Re and the Strouhal number *S*t, which are defined as:

$$U_r = \frac{U}{f_n D} \tag{7}$$

where U is the flow velocity, f_n is the natural frequency and D is diameter of the cylindrical buoyancy can.

$$\mathrm{Re} = \frac{UD}{\nu} \tag{8}$$

$$St = \frac{fD}{U} \tag{9}$$

where, f is the vortex-shedding frequency. f is taken as the cross-flow frequency f_y. Similarly, U is the flow velocity, D is diameter of the cylindrical buoyancy can. And ν is the fluid's kinematic viscosity coefficient.

The motion amplitude of the buoyancy can is expressed as dimensionless motion root-mean-square amplitude [1], defined as:

$$A^*_{RMS} = \frac{\sqrt{\frac{1}{N}\sum_{i=1}^{N}(x_i - \mu)^2}}{D} \tag{10}$$

where, x_i is the displacement of buoyancy can in a stable period, μ is the mean value of the displacement and D is diameter of the buoyancy can.

3.2 Computational Model

The computational model in this paper is the model in the towing experiment delivered by KANG et al. [6]. The model of the buoyancy can is in typical cylindrical shape and detail parameters of the buoyancy can are shown in Table 1.

As shown in Fig. 1, the overall buoyancy can is underwater regardless of the free surface issue. The buoyancy can is connected with a mooring line at the centre of the bottom of the model, fairlead point. And the anchor point is outside the computational domain.

3.3 Case Condition

In free decay test case, buoyancy can under no incoming flow is given an initial velocity of 0.2 m/s and released so that the model can be free to decay. While VIM test cases are carried out under uniform flow during a range of reduced velocities, from 4 to 10, and detail information is shown in the following Table 2.

Table 1 Parameters of the buoyancy can.

Parameter	Unit	Value
Outer diameter (D)	mm	150
Length (L)	mm	700
Displacement (△)	kg	12.37
Weight (w)	kg	4.24

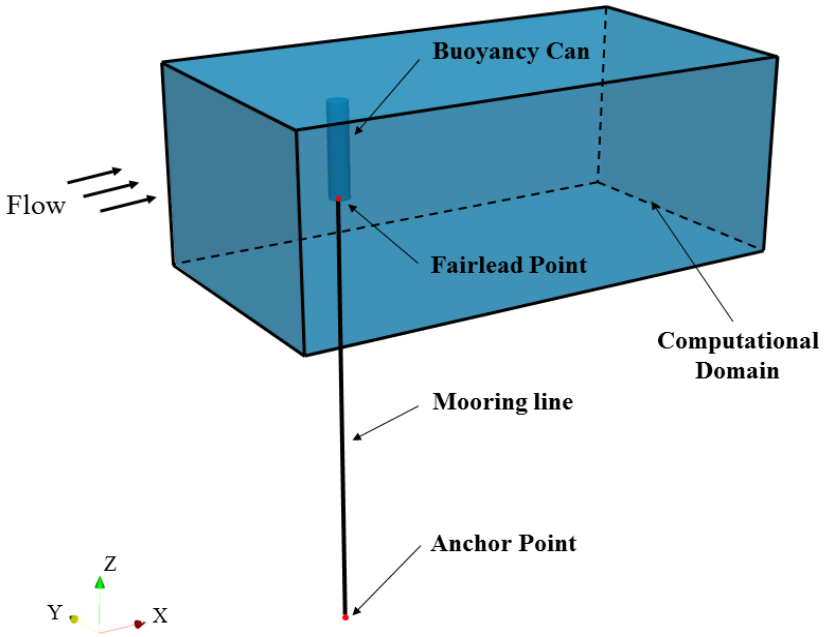

Fig. 1 Schematic diagram of computational model.

Table 2 VIM case condition.

Reduced velocity (U_r)	Flow velocity/m·s^{-1}	Re
4	0.128	1.68×10^4
6	0.192	2.52×10^4
7	0.223	2.94×10^4
8	0.255	3.36×10^4
10	0.319	4.20×10^4

3.4 Computational Domain, Mesh, Boundary Condition

The computational domain and the mesh are shown in Figs. 2 and 3. The length of the entire computational domain is 25D, the width is 12D, and the height is 10D. And the origin of the computational domain is set in the centre of the buoyancy can. The origin point is 5D from the upstream inlet, 20D from the downstream outlet, 6D from bottom face and 5D from the side face.

Since the overset grid is applied in the cases, there are two kinds of mesh, one is cylinder grid, the other is background grid illustrated in Fig. 3b. Both grids are structured grid and the vicinity of the cylinder is locally refined as Fig. 3a shows. In cylinder grid region, the grid size near the wall is set to be small to obtain more accurate flow separation and y+ is about 5. And the grid number of background grid region is 0.71 million, while that of cylinder grid region is 1.62 million. Fig. 3b shows the local mesh distribution of cylinder at the z = 0 section. The boundary conditions of the computational domain are set as follow: free stream velocity for inlet, pressure equals zero for outlet, symmetry for top, slip for other side patches.

4. Result and Discussion

4.1 Free Decay Test

In free decay test case, the buoyancy can under no incoming flow is given an initial velocity and released to get the natural period of the mooring system. Since the consecutive VIM numerical tests are under the condition that the length of mooring line is 2.672 m, the numerical free decay test keeps the same length of the mooring line. After the Fourier transform, it shows that the CFD result fits well with the KANG et al.'s [6] experimental result as Fig. 4 presents:

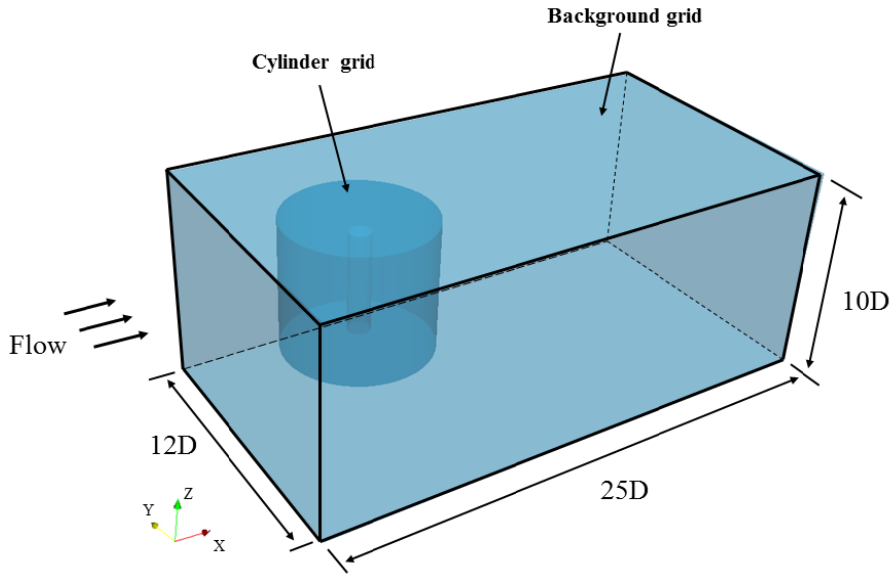

Fig. 2 Computational domain.

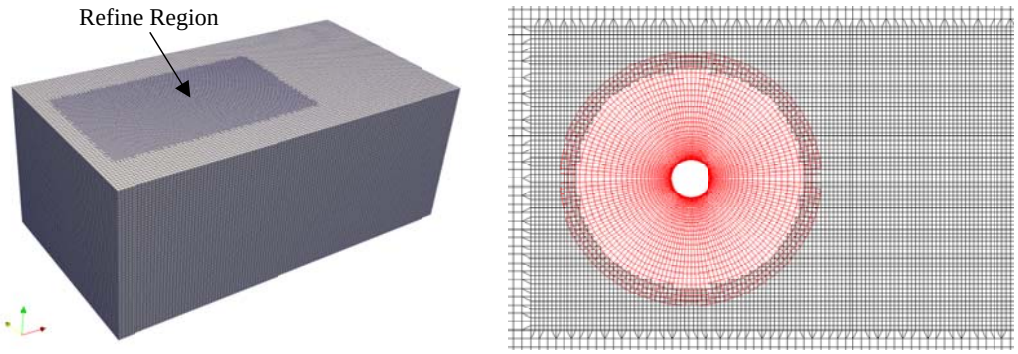

(a) Overall computational mesh (b) Local mesh

Fig. 3 Computational mesh.

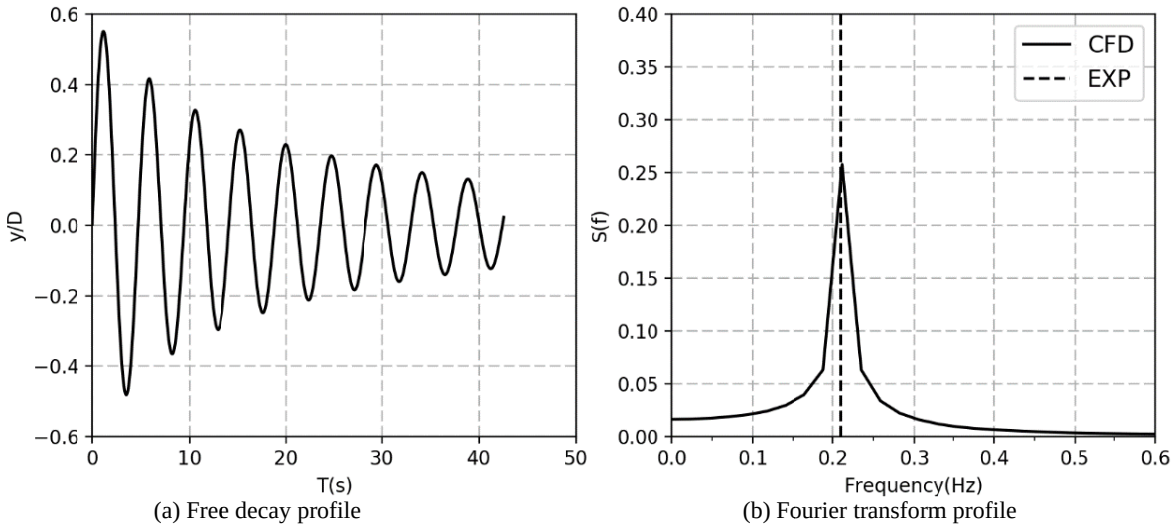

(a) Free decay profile (b) Fourier transform profile

Fig. 4 Tether length L = 2.672 m free decay result.

4.2 Motion Trajectory

The VIM numerical tests are delivered respectively at several reduced velocities (4/6/7/8/10), and Fig. 5 presents time-displacement, Fourier transform profiles and motion trajectories when reduced velocity equals to 4/6/8.

As shown in Fig. 5, when reduced velocity is equal to 4, sway motion is unstable, and the amplitude of the sway frequency is approximate with the surrounding frequency peaks. Furthermore, with the increase of reduced velocity, the average surge displacement and surge and sway frequency of the buoyancy can are increased significantly. In general, when the vortex shedding is stable, the motion trajectory becomes regular in “8” shape. The internal mechanism of the special shape is that the surge frequency is twice of the sway frequency just as Fig. 6 presents.

Fig. 6 shows f_x/f_n, f_y/f_n, f_x/f_y of the cylinder versus reduced velocity U_r, where f_n is the natural frequency, f_x is the surge frequency, f_y is the sway frequency. From the trend of these points, it can be obtained that the ratio of the surge and the sway frequency is around 2 and the sway and surge frequency is increased with the reduced velocity, which conforms to the VIM mechanism. In addition, “lock-in” phenomenon is not observed in these cases. The low mass ratio (mass ratio = 0.343) and only five cases in this paper may be the dominant reasons for this circumstance, and further studies should be delivered in this part.

4.3 Yaw Motion

In this paper, this numerical method can obviously capture the rotation phenomenon of the buoyancy can in the uniform flow. And the rotational frequency increases with the increase of the reduced velocity. From Fig. 7a, when the reduced velocity is low, the obvious dominant frequency cannot be found in Fourier transform, which is different from Fig. 7b and 7c. This phenomenon may be caused by the unstable vortex shedding. When the vortex shedding is unstable, it is hard to form a stable moment to keep the cylinder rotate, so the dominant frequency cannot be observed in low reduced velocity.

According to Table 3, same as surge and sway frequency, the yaw frequency increases with the increase of reduced velocity. Secondly, yaw frequency is equal to the sway frequency, which is consistent with KANG et al.’s [6] experimental result. The reason for this circumstance is that the sway motion and yaw motion are both caused by the vortex shedding. It can infer that the sway motion and yaw motion share the same exciting force component.

After that, two cases, one fixed in rotation and the other one free in rotation when reduced velocity equals to 7 are carried out.

In Fig. 8, whether to release the degree of rotation shows no difference in time series profile, but it indicates that the release in degrees of rotation induces the earlier stable vortex shedding of a buoyancy can. Furthermore, the RMS of the surge and sway motion amplitudes are calculated in Table 4.

In Table 4, it indicates that release in the degree of rotation can decrease the sway amplitude, while this change makes no difference in the surge amplitude, which conforms to the two dimensional numerical result of Etienne et al. [8]. However, in his work, the decrease in sway motion is more obvious than that of the present work. The reason for this difference may be that 3D flow is much more complicated than the 2D flow and the vortex shedding in the free end of the buoyancy can may affect the yaw motion.

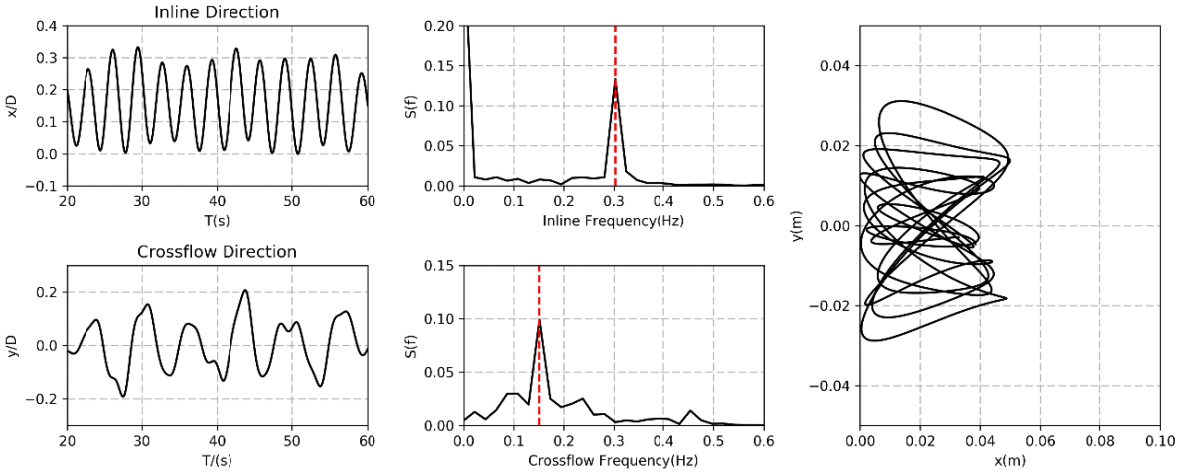

(a) $U_r = 4$

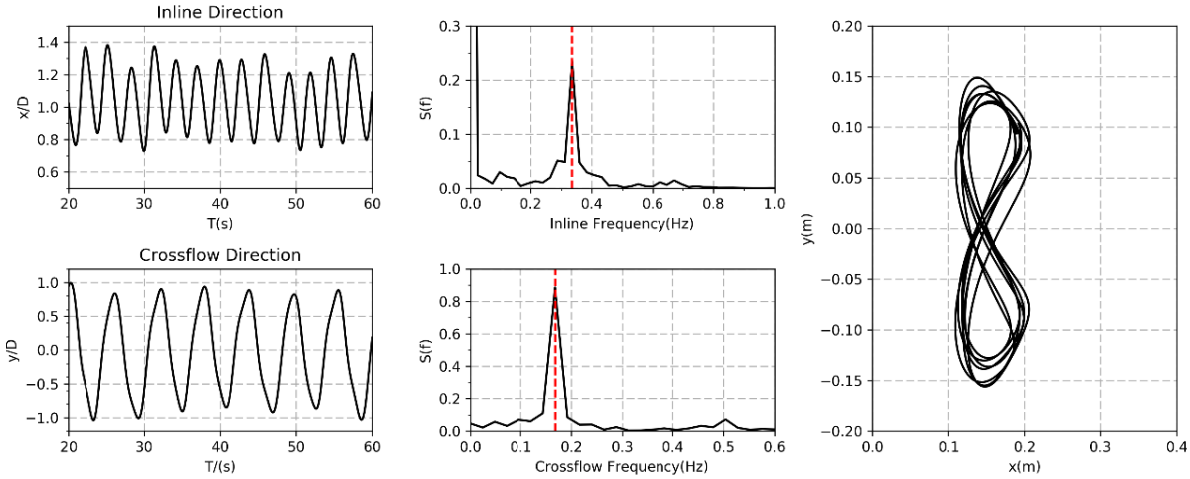

(b) $U_r = 6$

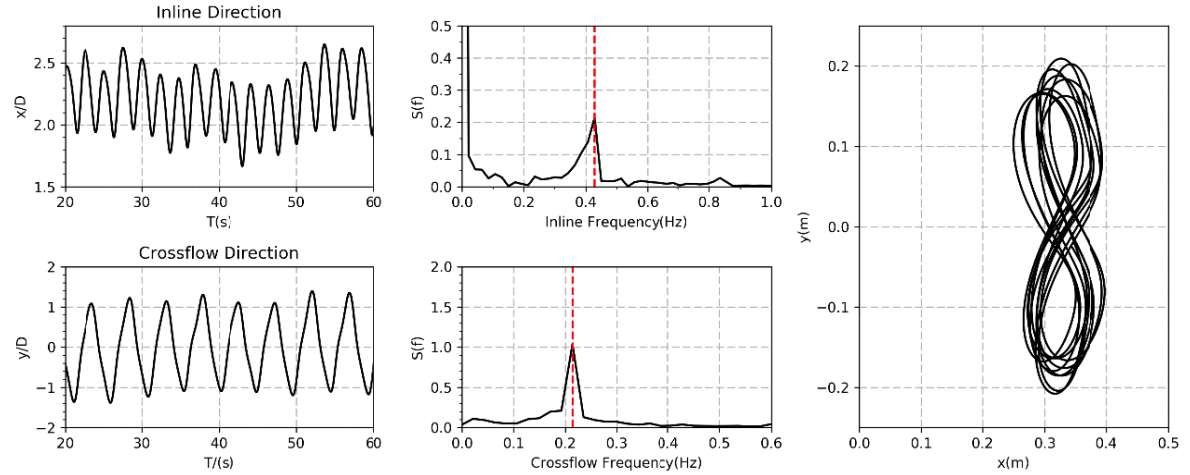

(c) $U_r = 8$

Fig. 5 Time-Displacement profile & Fourier transform profile & Motion trajectory.

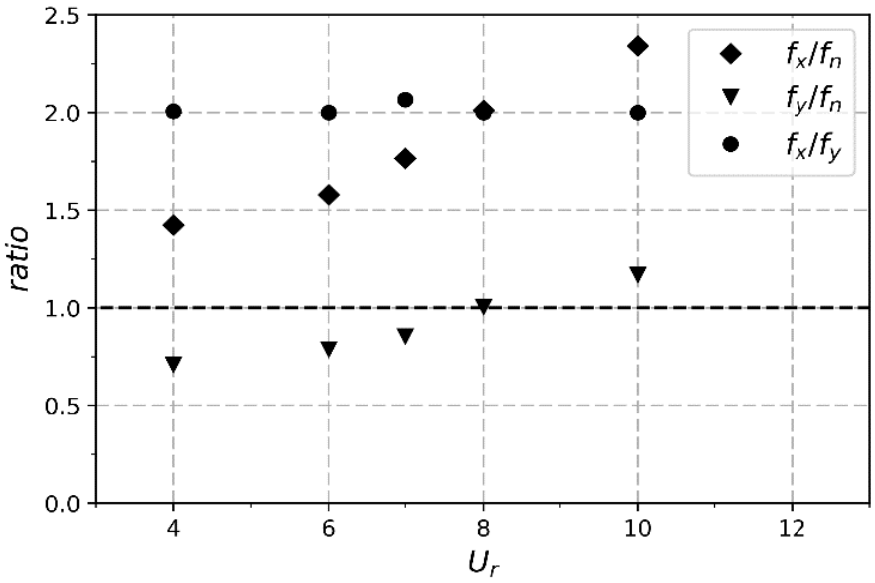

Fig. 6 VIM frequency of the buoyancy can.

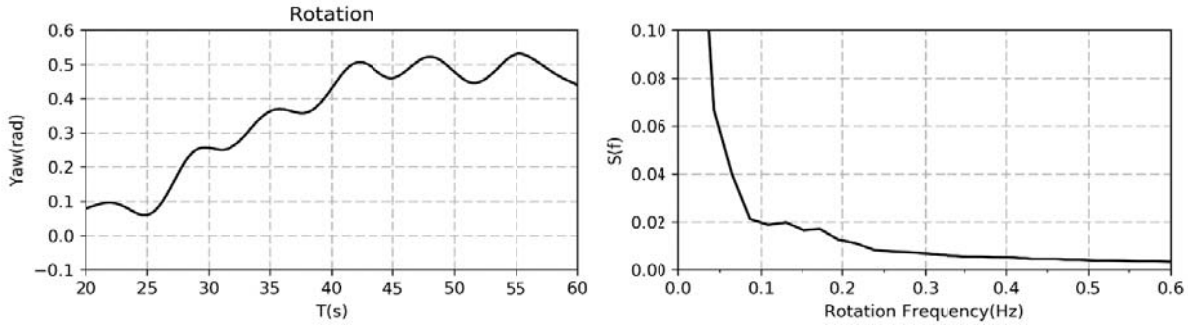

(a) $U_r = 4$

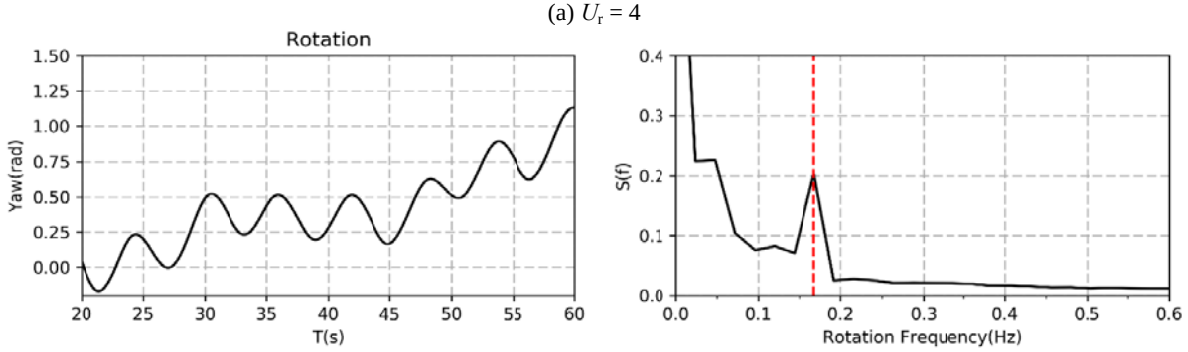

(b) $U_r = 6$

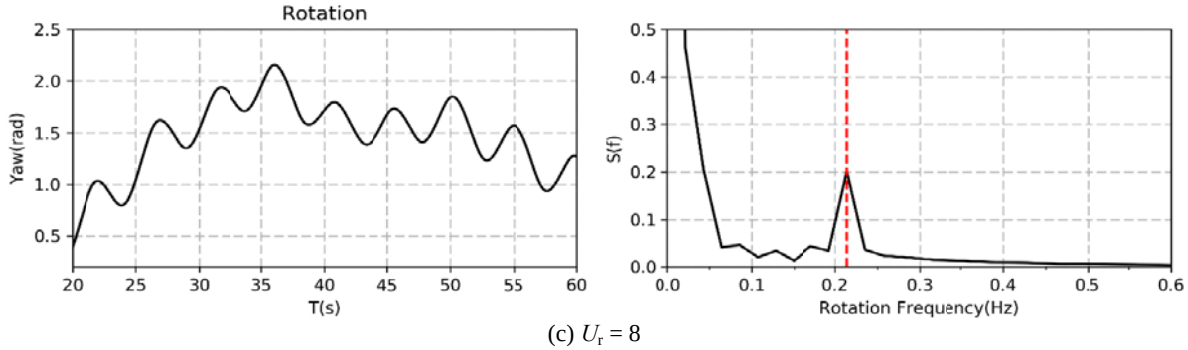

(c) $U_r = 8$

Fig. 7 Time-rotation profile & Fourier transform profile.

Table 3 Surge frequency, sway frequency and yaw frequency.

Reduced velocity (U_r)	Surge frequency/Hz	Sway frequency/Hz	Yaw frequency/Hz
4	0.303	0.151	-
6	0.336	0.168	0.168
7	0.376	0.182	0.182
8	0.428	0.214	0.214
10	0.498	0.249	0.249

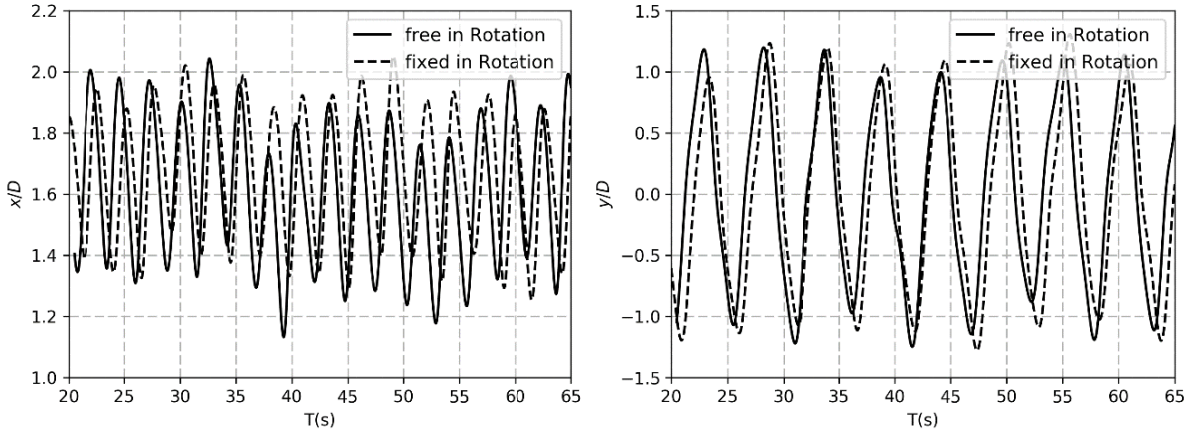

Fig. 8 Dimensionless sway and surge amplitude in time series.

Table 4 Surge and sway amplitude RMS in U_r = 7.

Case	Free in rotation	Fixed in rotation
Surge amplitude RMS	0.218	0.215
Sway amplitude RMS	0.747	0.765

5. Conclusions

This paper presents 3D CFD simulation to analyse the FIR especially the yaw motion of a buoyancy can. The numerical tests are conducted with a buoyancy can under different reduced velocities utilizing naoe-FOAM-SJTU including SST-DDES model and oversets grid method. The following conclusions are made:

The numerical model in this paper can predict the free decay test and VIM test well with the experiment. And in VIM cases, with the increase of the reduced velocity, the stable vortex shedding can be observed in result and the motion trajectory becomes regular in “8” shape.

The yaw frequency increases with the increase of reduced velocity, which is similar to surge and sway frequency. And yaw frequency is equal to the sway frequency, which implies that the sway motion and yaw motion share the same exciting force component.

In the state of Reynolds number equal to 2.94×10^4, the rotational degree of freedom in buoyancy can can slightly decrease the RMS of sway amplitude in 2.41% but make no difference to the RMS of surge amplitude.

The future work includes the study of the influence of rotating damping and the mechanism of vortex-induced rotation. And in this paper Reynolds number is around 10^4, high Reynolds numerical test will also be set in the future work.

Acknowledgements

This work is supported by the National Natural Science Foundation of China (51490675, 51379125, 11432009, 51579145), Chang Jiang Scholars Program (T2014099), Shanghai Excellent Academic Leaders Program (17XD1402300), Shanghai Key Laboratory

of Marine Engineering (K2015-11), Program for Professor of Special Appointment (Eastern Scholar) at Shanghai Institutions of Higher Learning (2013022), Innovative Special Project of Numerical Tank of Ministry of Industry and Information Technology of China (2016-23/09) and Lloyd's Register Foundation for doctoral student, to which the authors are most grateful.

References

[1] Karunakaran, D., Lee, D., and Mair, J. 2009. "Qualification of the Grouped SLOR Riser System." In *Proceedings of the Offshore Technology Conference*, 4-7.

[2] Irani, M., and Finn, L. 2004. "Model Testing for Vortex Induced Motions of Spar Platforms." In *Proceedings of the ASME 2004 23rd International Conference on Offshore Mechanics and Arctic Engineering,* 605-10.

[3] Oakley, O. H., Navarro, C., Constantinides, Y., and Holmes, S. 2005. "Modeling Vortex Induced Motions of Spars in Uniform and Stratified Flows." In *Proceedings of ASME 2005 24th the International Conference on Offshore Mechanics and Arctic Engineering,* 885-94.

[4] Govardhan, R., and Williamson, C. H. K. 1997. "Vortex-Induced Motions of a Tethered Sphere." *Journal of Wind Engineering and Industrial Aerodynamics* 69-71: 375-85.

[5] De Wilde, J. 2007. "Model Tests on the Vortex Induced Motions of the Air Can of a Free Standing Riser System in Current." In *Proceedings of the Deep Offshore Technology Conference,* 1-10.

[6] KANG, Z., NI, W. C., MA, G., and XU, X. 2017. "A Model Test Investigation on Vortex-Induced Motions of a Buoyancy Can." *Marine Structures* 53: 86-104.

[7] KANG, Z., NI, W. C., ZHANG, X., and SUN, L. P. 2016. "An Experimental Investigation of Six-Degrees-of-Freedom VIM Characteristics of a Tethered Buoyancy Can." In *Proceedings of the Twenty-sixth International Ocean and Polar Engineering Conference,* 1109-15.

[8] Etienne, S., and Fontaine, E. 2010. "Effect of Rotational Degree of Freedom on Vortex-Induced Vibrations of a Circular Cylinder in Cross-Flow." In *Proceedings of the 20th International Offshore and Polar Engineering Conference,* 20-5.

[9] Minguez, M., Luppi, A., and Berger, A. 2012. "Slender Buoy FSHR Vortex Induced Rotations." In *Proceedings of the ASME 31st International Conference on Ocean, Offshore and Arctic Engineering,* 713-22.

[10] Minguez, M., Luppi, A., Pattedoie, S., and Maloberti, R. 2011. "Slender Buoy VIM and VIR Analysis by CFD/FSI Approach." In *Proceedings of the ASME 30th International Conference on Ocean, Offshore and Arctic Engineering,* 1-9.

[11] ZHAO, W. W., and WAN, D. C. 2016. "Detached-Eddy Simulation of Flow past Tandem Cylinders." *Applied Mathematics and Mechanics* 37 (12): 1272-81.

[12] Menter, F. R., Kuntz, M., and Langtry, R. 2003. "Ten Years of Industrial Experience with the SST Turbulence Model." In *Proceedings of the 4th International Symposium on Turbulence Heat and Mass Transfer,* 625-32.

[13] Noack, R., David, B., Robert, K., and Pablo, C. 2009. "Suggar++: An Improved General Overset Grid Assembly Capability." In *Proceeding of the 19th AIAA Computational Fluid Dynamics,* 22-5.

[14] SHEN, Z. R., and WAN, D. C. 2012. "The Manual of CFD Solver for Ship and Ocean Engineering Flows: Naoe-FOAM-SJTU." Shanghai, China: Shanghai Jiao Tong University.

[15] SHEN, Z. R., and WAN, D. C. 2013. "RANS Computations of Added Resistance and Motions of a Ship in Head Waves." *International Journal of Offshore and Polar Engineering* 23 (4): 263-71.

[16] SHEN, Z. R., WAN, D. C., and Pablo M. C. 2015. "Dynamic Overset Grids in Open FOAM with Application to KCS Self-propulsion and Maneuvering." *Ocean Engineering* 108: 287-306.